Supporting information

Defect-Engineered Pd/WO_{3-x} Nanostructures with Tunable Morphology for Enhanced Visible-NIR Light-Driven Catalysis

Priyanka,[a] Rashmi,[a] Hideyuki Kawasoko,[b] Soichi Kikkawa,[b] Seiji Yamazoe,[b] Ryo Watanabe,[c] Choji Fukuhara,[c] and Priyanka Verma[a,*]

[a]*Department of Chemistry, Indian Institute of Technology Delhi, Hauz Khas, New Delhi 110016, India Email: pverma@chemistry.iitd.ac.in*

[b]*Department of Chemistry, Graduate School of Science, Tokyo Metropolitan University, 1-1 Minami-Osawa, Hachioji, Tokyo 192-0397, Japan*

[c]*Department of Applied Chemistry and Biochemical Engineering, Graduate School of Engineering, Shizuoka University, 3-5-1 Johoku, Chuo-ku, Hamamatsu, Shizuoka 432-8561, Japan*

Synthesis and purification of PVP-stabilized palladium nanoparticles

0.557 g (5 mmol) of polyvinylpyrrolidone (PVP) was dispersed in 60 mL of ethylene glycol to obtain a clear solution, which was then stirred at 80 °C for 2 hours. Subsequently, the solution was cooled to 0 °C, followed by the addition of 3 mL of 1 M NaOH solution. In parallel, a separate solution was prepared by dissolving 0.11225 g (0.5 mmol) of palladium acetate ($Pd(OAc)_2$) in 25 mL of dioxane, resulting in an orange-colored solution that was stirred at room temperature for 2 hours. The two solutions were then combined and stirred at 100 °C for 2 hours, producing a dark brown colloidal dispersion. After cooling to room temperature, the palladium nanoparticles were purified by adding excess acetone to induce flocculation and polymer removal. The mixture was vigorously shaken, and the organic phase was separated. Finally, the purified Pd nanoparticles were redispersed in methanol for further use. For better clarity and understanding, a stepwise schematic representation has been provided, as displayed in **Fig. S1**.

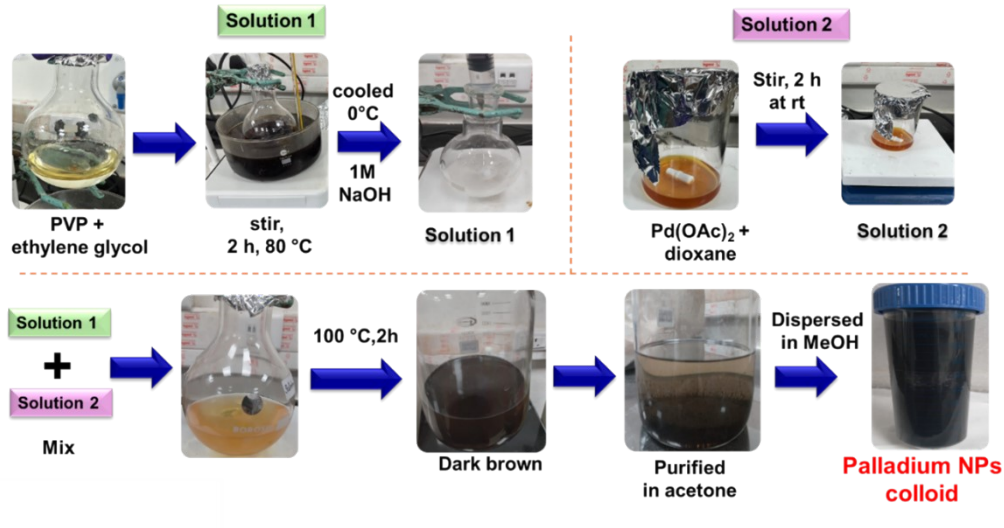

Fig. S1 Schematic representation of the synthesis of Pd colloidal solution.

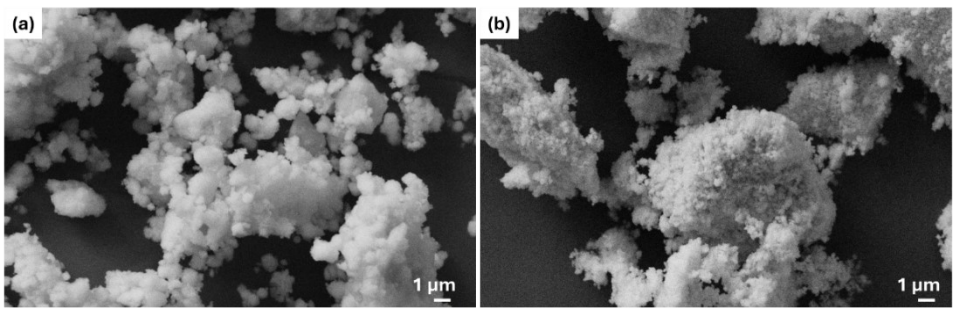

Fig. S2 SEM images of (a) Pd/WO_{3-x}, and (b) Pd/Commercial WO_3.

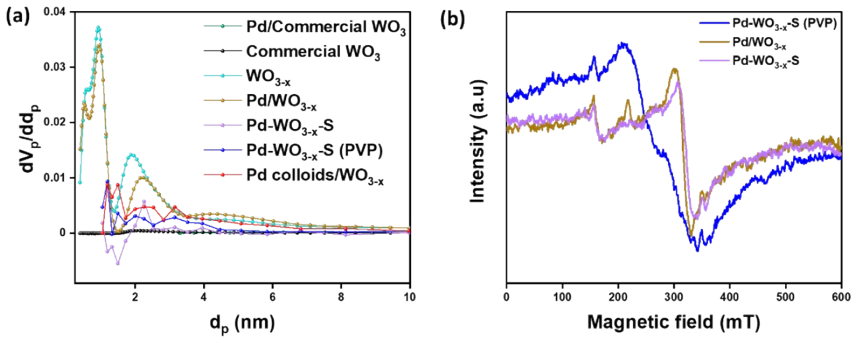

Fig. S3 (a) BJH pore size distribution for all samples (b) EPR spectra of Pd-WO_{3-x}-S (PVP), Pd/WO_{3-x} and Pd-WO_{3-x}-S measured at room temperature conditions.

Table S1. Comparison of BET surface area, pore size, and pore volume of prepared catalysts.

Samples	Comm. WO_3	WO_{3-x}	Pd/WO_{3-x}	Pd colloids/WO_{3-x}	Pd-WO_{3-x}-S	Pd-WO_{3-x}-S (PVP)	Pd/WO_3
BET surface area (m^2g^{-1})	2.0317	66.51	56.826	22.2	1.5342	15.858	1.523
Total pore volume(cm^3g^{-1})	0.0030	0.056	0.0520	0.0041	0.0041	0.0043	0.0562

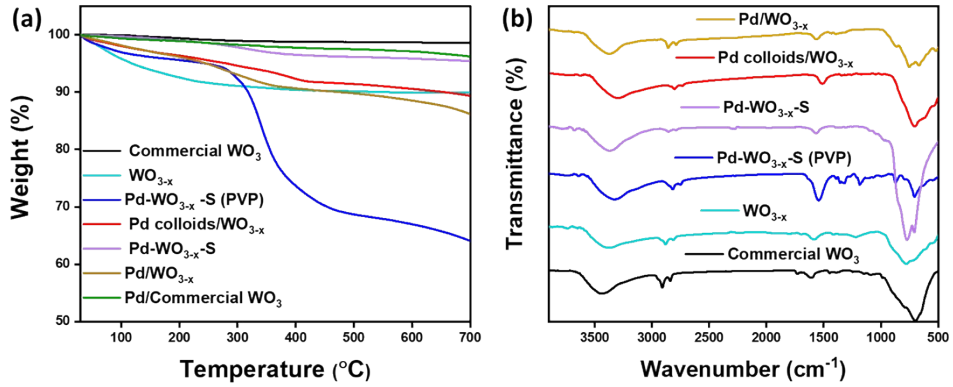

Fig. S4 (a) Thermogravimetric analysis curves of commercial WO_3, WO_{3-x}, and all Pd-deposited WO_{3-x} samples (b) FT-IR spectra of all synthesized samples.

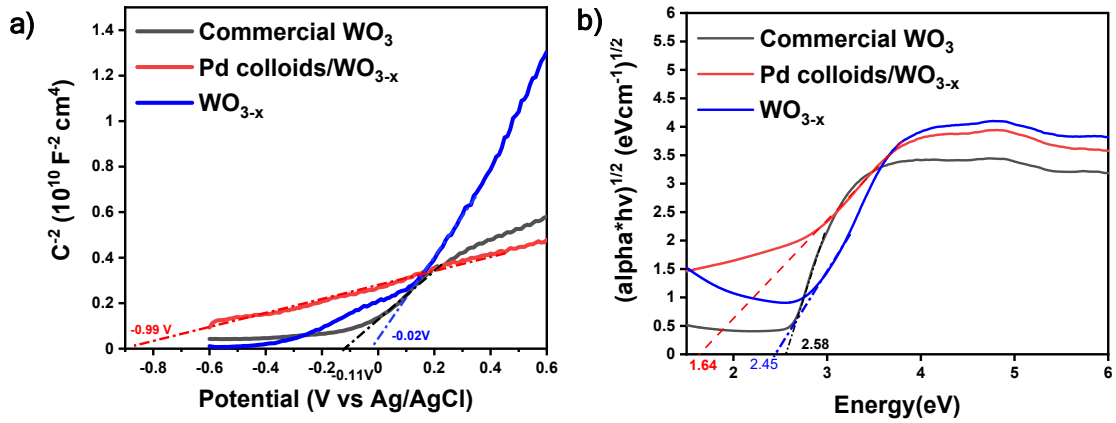

Fig S5. (a) Mott–Schottky plot and (b) Tauc plot for commercial WO_3, WO_{3-x} and Pd colloids/WO_{3-x}.

XPS Analysis: In commercial WO_3, the W 4f spectrum exhibits two prominent peaks at 35.7 and 37.8 eV, corresponding to W $4f_{7/2}$ and W $4f_{5/2}$, respectively, attributable to the W^{6+} oxidation state **Fig. S6 (a)**. A minor contribution of W^{5+} at slightly lower binding energies was also observed, though the spectrum is predominantly indicative of W^{6+} species. It is well known that the introduction of oxygen vacancies increases the electron density around metal centres, leading to a reduction in binding energy. As shown in **Fig. S6 (b)**, the W 4f spectrum of WO_{3-x} displays doublet peaks at 34.7 and 36.9 eV (W^{5+}) and 35.7 and 37.8 eV (W^{6+}), confirming the presence of oxygen vacancies. **Fig. S6 (c)** shows the W 4f XPS spectrum of Pd/WO_{3-x}, which also exhibits dominant W^{6+} peaks (at 36.0 and 38.1 eV) along with lower binding energy peaks assigned to W^{5+}(at 34.6 and 36.7 eV), indicating the retention of oxygen defects after Pd deposition. The Pd 3d XPS spectrum shown in **Fig. S6 (d)** reveals peaks at 337.7 eV (Pd $3d_{5/2}$)and 342.8 eV (Pd $3d_{3/2}$), characteristic of metallic Pd^0, with negligible oxidized Pd species detected.

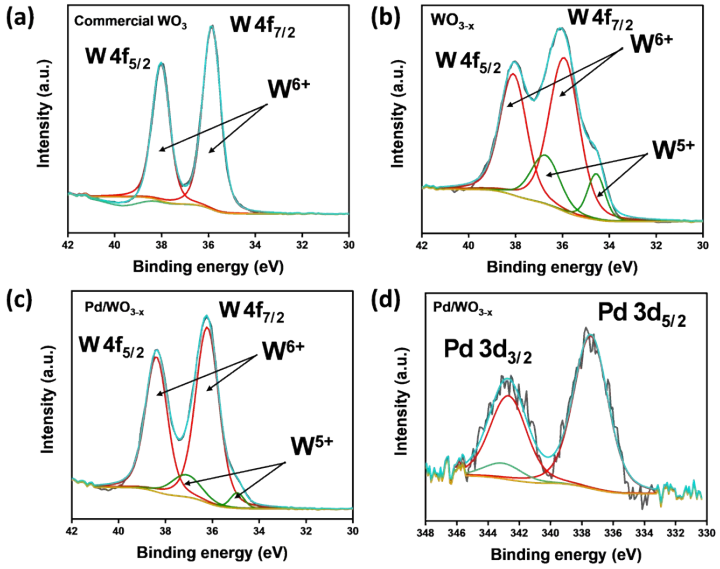

Fig. S6 W 4f XPS spectrum of (a) Commercial WO_3, (b) WO_{3-x}, (c) Pd/WO_{3-x} and (d) Pd 3d XPS spectra of Pd/WO_{3-x}.

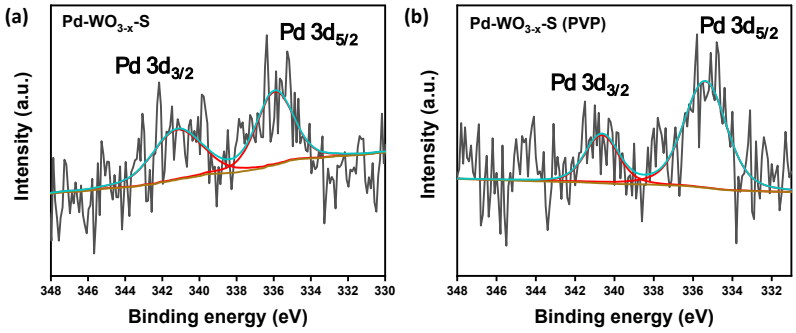

Fig. S7 The Pd 3d spectrum of (a) Pd-WO_{3-x}-S and (b) Pd-WO_{3-x}-S (PVP).

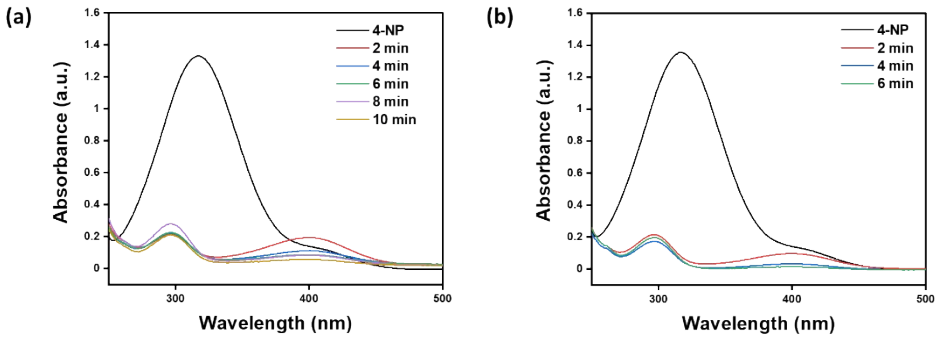

Fig. S8 Photocatalytic reduction of 4-nitrophenol (4-NP) for Pd colloids/WO_{3-x} in (a) dark and (b) under light irradiation conditions. Reaction conditions: 5 mg catalyst, 10 mL water, 7 mM 4-NP, 5 mL of 0.025 M AB solution, and 300 W Xenon lamp.

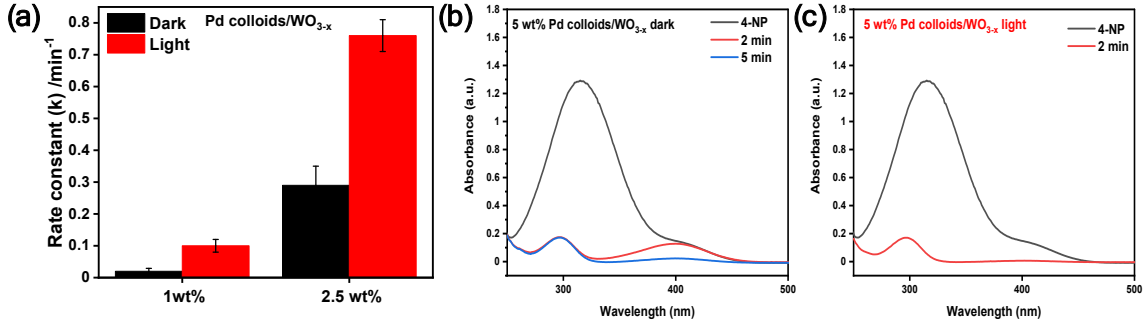

Figure S9: (a) Rate constant comparison between 1.0 wt% & 2.5 wt% (b, c) Reaction kinetics plot for 5.0 wt% Pd colloids/WO_{3-x} in dark and under light irradiation conditions.

Table S2. Comparative summary of reported plasmonic photocatalysts and their kinetic performance toward 4-NP reduction.

S.No.	Catalytic	Initial concentration (mM)/ light source	Catalyst amount (g/L)	Reducing agent	Rate constant (min^{-1})	References
1	$Ag@Ag_2S/WO_3$	1.8×10^{-4}, Mercury lamp (160 W)	1.0	$NaBH_4$	7.3×10^{-3}	1
2	Ag/WO_x	10	0.083	$NaBH_4$	0.18	2
3	Ni/WS_2	0.05	2.5	$NaBH_4$	0.31	3
4	WO_3 nanoplates	20, MH lamp	1.0	--	0.510	4
5	$Au@MoO_{3-x}$	0.1, Xenon lamp	70 µL	$NaBH_4$	0.15	5
6	TiO_2-Mo	0.2156, UV lamp	1.0	--	0.182	6
7	Pd/MoO_3 H_2-RT	0.2, Visible light (λ >420 nm)	0.167	NH_3BH_3	0.039	7
8	Pd/WO_{3-x}	7.0, Xenon lamp (300 W)	0.33	NH_3BH_3	0.75	This work

References:

(1) E. Torad, E. H. Ismail, M. M. Mohamed, M. M. H. Khalil, *Mater. Res. Bull.*, 2021, **137**, 111193.

(2) Z. Wu, X. Lü, X. Wei, J. Shen, J. Xie, *J. Mater. Res.*, 2014, **29**, 71–77.

(3) R. Das, R. Kakati, A. Kumari, S. Vaidya, A. Baruah, *Environ. Sci. Pollut. Res.*, 2025, **44**, 25155-25171.

(4) A. Zarei, F. Hedayatinasab, H. Rezaei-Vahidian, *Environ. Prog. Sustain. Energy*, 2020, **39**, e13386.

(5) Z. Tao, J. Feng, F. Yang, L. Zhang, H. Shen, Q. Cheng , L. Liu, *Nanotechnology*, 2023, **34**, 154001.

(6) R. López, R. Gómez, *Top. Catal.*, 2011, **54**, 504–511.

(7) H. Cheng, M. Wen, X. Ma, Y. Kuwahara, K. Mori, Y. Dai, B. Huang, H. Yamashita, *J. Am. Chem. Soc.*, 2016, **138**, 9316–9324.